Journal of Testing and Evaluation, Vol. 37, No. 6
Paper ID JTE101574
Available online at: www.astm.org

Ph. P. Darcis,[1] *J. M. Treinen,*[1] *and J. D. McColskey*[1]

Fatigue Crack Growth Rates in Pipeline Steels Using Curved M(T) Specimens*

ABSTRACT: This study presents fatigue data for two different ferrite-pearlite pipeline steels. A fatigue crack growth test for full-thickness curved pipeline samples was developed using a middle tension (M(T)) specimen. Also, finite element analyses (FEAs) were carried out to show the M(T) curvature effects on the fatigue crack growth results. The two steels showed similar fatigue crack growth rate (*da*/*dN*) behavior. However, the ferrite-pearlite steel without banding had slightly better fatigue properties than the ferrite-pearlite banded steel. Uncertainty in the fatigue crack growth rates was analyzed by attributing all the fatigue scatter to the Paris law parameter *C*. The FEA based simulations, based on curved geometries, of the compliance relationship more accurately predicted both fatigue crack growth data and true crack lengths. Nevertheless, the ASTM E647-05 compliance relationship accurately predicted the crack length for the M(T) geometry, although its use leads to slightly conservative fatigue crack growth trends and a slight overestimation of the true final crack length.

KEYWORDS: crack length measurement, curved middle tension specimen, fatigue crack growth

Introduction

The expanding need for oil and gas transportation places new requirements on the steels used in large-diameter pipelines. It is well established that early damage may initiate in service fatigue cracking, generated by the fluctuations in the internal operating pressure, as well as by the variation in external loads. The fatigue crack growth can be accelerated by an aggressive environment [1–3].

Therefore, the safety assessment of gas and oil pipelines must take fatigue properties into consideration [1,4,5]. Fatigue, recognized as an important mechanical property, has been included in both U.S. pipeline integrity management regulations and multinational design standards [6–9].

The most common method of estimating fatigue life and inspection times is to employ a linear-elastic fatigue crack growth expression based on the "Paris law" relationship

$$\frac{da}{dN} = C(\Delta K)^m, \tag{1}$$

where:

da/dN(mm/cycle) = increment in crack growth per cycle,
C and m = material properties, and
ΔK (MPa·mm$^{1/2}$) = variation in stress intensity factor.

By choosing the Paris law, the present study limits the application of this work to the region II of the fatigue crack growth rate (FCGR) curve and neglects the stress ratio and load sequence effects. The loading effect study, like the overloads, the underloads, and the change in the FCGR as a function of the loading ratio, was not the intent of the present paper. Trends similar to those presented here could be expected with different load ratios under constant amplitude loading.

To use this approach, one must determine both the initial crack size and the final crack size that will cause failure in service. In addition, one must apply relevant crack growth rate characteristics for the material (the C and m values in the Paris law equation) and a representative operating pressure spectrum for the pipeline of interest in order to calculate the times to failure for the various credible defect sizes. Finally, one should apply a factor of safety to the minimum calculated time to failure to account for inaccuracies in the methodology and random errors in the variables to make certain that intervention can take place before a failure occurs [8,9].

In the present work the FCGR evaluation is investigated. The common way to monitor FCGR tests is to use a clip gage mounted in the specimen notch and calculate the crack length using the specimen compliance via the crack mouth opening displacement (CMOD). This method has the advantage of generating data directly during the fatigue test without any stop-and-start process, and it is based entirely on the compliance relationship. This relationship is the key to the accuracy of the entire test and will be discussed in this paper.

The possible effects of using curved specimens machined directly from the full-thickness pipeline are also examined. The pipeline industry usually uses flattened or machined small-size specimens, such as single-edge notched [5,10–12], compact tension (C(T)) [3,13,14], or three-point bending [15] specimens, to assess FCGR material properties. This leads to three limitations.

(1) Small specimens, with a short fatigue crack growth ligament, are not ideal to identify FCGR parameters in pipelines of large diameters.
(2) Using flattened specimens manufactured from the new thermomechanically controlled process (TMCP) technique induces a Bauschinger effect and changes the material properties of the investigated pipeline steel [16].
(3) Using surface machined specimens eliminates the surface effect on the pipeline, which is sensitive to the TMCP process, and eliminates the effect of pipeline coating, if present, on FCGR.

A way to avoid these specimen effects is to use a full-thickness center-cracked middle tension (M(T)) specimen, which is designed specifically for FCGR measurements and is directly machined from

Manuscript received November 28, 2007; accepted for publication May 28, 2009; published online July 2009.

[1]Materials Reliability Division, NIST, 325 Broadway, Boulder, CO 80305-3328.

TABLE 1—*Designation of the tested steels.*

Designation	OD (in.)	OD (m)	Thickness (mm)
X52	20	0.51	8.1
Grade B	22	0.56	7.4

TABLE 4—*Measurements (mean) of the metallurgical features.*

Steel	Ferritic Grain Size (μm)	Pearlite Volume Fraction (%)
X52	11.8	37.1
Grade B	10.8	25.3

the pipeline without any surface machining (grinding) or flattening.

In this paper, a curved M(T) test setup is presented, and finite element analyses (FEAs) are carried out to show the M(T) curvature effects on the compliance relationship and on the FCGR results for two different pipeline steels.

Material Properties

Two pipeline steels that were removed from service were tested. The steels were API X52 and API Grade B low-strength pipeline steels. Table 1 summarizes the pipe dimensions.

Nominal chemical compositions of the selected steels are given in Table 2. As shown, these steels contain high carbon as well phosphorus and sulfur.

To measure the tensile properties of pipeline steels, flat tensile specimens (6 mm wide) were machined from the pipeline. Those taken in a longitudinal orientation (axial orientation) were full thickness. The circumferential specimens were 3 mm thick, and no tests were performed on the through-thickness orientation. All specimens had a uniform test section gauge length of 25.4 mm. Experiments were performed in a screw-driven tensile testing machine of 100 kN capacity, and a closed-loop servohydraulic machine of 100 kN capacity. Tests were conducted in displacement control at a rate of 0.25 mm/min. Two tests were conducted for the circumferential (C) direction and two for the longitudinal (L, direction of maximum grain flow) direction for each steel. The mean mechanical properties measured for the two steels are shown in Table 3; E is the Young's modulus, $\sigma_{0.2}$ is the yield strength, σ_{UTS} is the ultimate strength, e_u is the uniform elongation, and e_f is the fracture elongation. Table 4 lists some measurements of the metallurgical features.

These steels had been in service for many years, and Young's modulus (calculated from the stress-strain curves) on full-thickness specimens is subject to specimen effects such as surface irregularities and corrosion. Dynamic elastic modulus measurements for the samples taken from these two pipeline steels were conducted according to standard ASTM E1876-07 [17]. Table 5 summarizes three dynamic elastic modulus measurements: $E(1)$, measured for out-of-plane flexure, which has the greatest strains on the wide flat sides; $E(2)$, measured for in-plane flexure, which has the greatest strains on the long edges; and $E(3)$, measured for longitudinal vibrations with equal strains across the cross section. For each steel, one dynamic elastic modulus test was conducted. The results show good correspondence between the steels, as might be expected.

Figure 1(*a*) and 1(*b*) illustrates the microstructures of the various steels, which emphasize the following points:

(a) steel X52 (Fig. 1(*a*)) is characterized by a ferrite-pearlite banded structure, and
(b) steel Grade B (Fig. 1(*b*)) is ferrite-pearlite steel without banding.

Experimental Procedures

Fatigue tests were conducted on M(T) specimens, as defined in ASTM E647-05 [18] machined from the longitudinal orientation with respect to the pipe axis, corresponding to the L-C orientation agreement with the ASTM E1823-05a [19]. Full-thickness specimens were tested with no flattening; only the portions of the specimen where the crack growth occurred were polished in order to optically verify the crack length. Specimen geometry, as defined in ASTM E647-05, and dimensions are depicted in Fig. 2. A through-thickness notch with a tip radius of 0.254 mm (0.01 in.) was introduced by spark erosion. Due to the specimen curvature, special adapters (Fig. 3) were designed to allow application of a uniform pressure by the hydraulic grips without deforming the specimen (the adaptors were pin mounted to the specimens to avoid sliding at the adaptor/specimen interface). To avoid introducing bending into the gage section, the centroid of the central specimen part, with a length of 208 mm in Fig. 2(*a*), corresponds to the centroid of the extremity test setup, specimen plus adapters; this assures the alignment of the specimen in the fatigue test machine. A special CMOD gauge was mounted directly across the notch opening, on the outer pipeline diameter, for monitoring the compliance (Fig. 4). The stan-

TABLE 2—*Chemical composition of the tested steels (wt %).*

Steel	C	Mn	P	S	Si	Cr	Ni	Cu	V	Nb	Mo	Co
X52	0.24	1.03	0.016	0.013	0.057	0.024	0.064	0.038	0.002	0.007	0.016	0.025
Grade B	0.27	0.36	0.005	0.015	0.009	0.029	0.021	0.015	0.003	0.005	0.007	0.007

TABLE 3—*Mechanical properties (mean).*

Steel	Orientation	E (GPa)	$\sigma_{0.2}$ (MPa)	σ_{UTS} (MPa)	$\sigma_{0.2}/\sigma_{UTS}$	e_u (%)	e_f (%)	e_u/e_f
X52	L	211.1[a]	380	556	0.68	11.6	32.7	0.38
	C	N/A	453	574	0.79	11.1	25.6	0.43
Grade B	L	212.1[a]	242	450	0.53	20.5	37.8	0.52
	C	N/A	254	458	0.55	18.5	38.0	0.49

[a]Average of the dynamic elastic modulus.

TABLE 5—*Three dynamic elastic modulus measurements.*

Steel	$E(1)$ (GPa)	$E(2)$ (GPa)	$E(3)$ (GPa)
X52	210.9	212.8	209.6
Grade B	213.3	211.5	211.5

dard equation for finding the crack length of a M(T) specimen from compliance data uses a fourth-order polynomial. This standard equation is from ASTM E647-05 [18] and will be presented later. To achieve a better measurement of the compliance, the top and bottom portions of the CMOD vs load curve were excluded, with only the interior points fitted. This should prevent nonlinearities encountered through phenomena such as crack closure from affecting the slope of the curve. Furthermore, points were collected on both sides of the loading and unloading curves in order to average possible hysteresis effects.

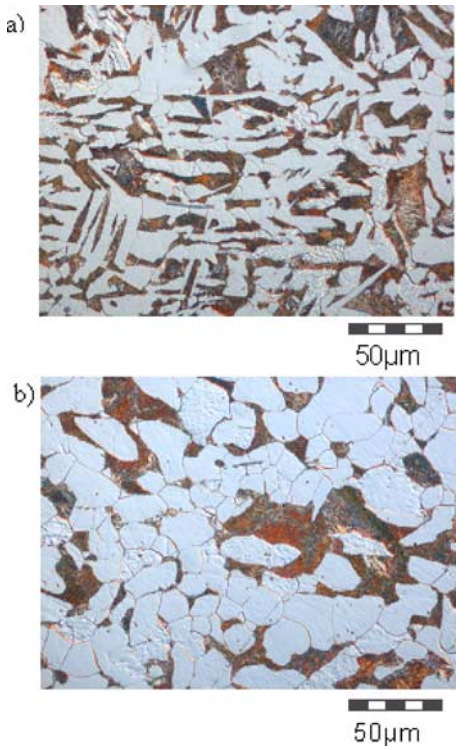

FIG. 1—*Microstructure of the steels (cross section parallel to the direction of rolling and L-C orientation (specimen length)): (a) steel X52 and (b) steel Grade B.*

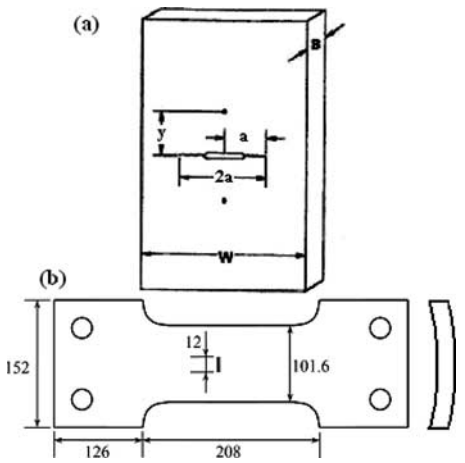

FIG. 2—*(a) ASTM E647-05 M(T) specimen characteristics [18] and (b) M(T) specimen dimensions (in mm).*

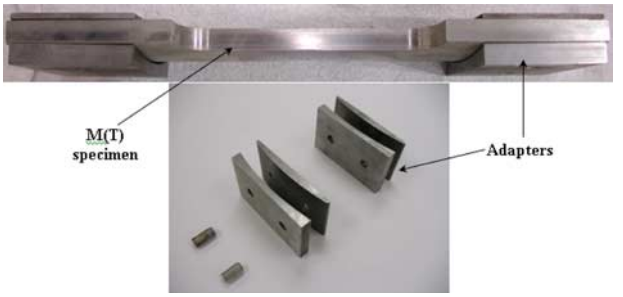

FIG. 3—*Special adapters designed for the M(T) curved specimen.*

The fatigue tests were conducted at room temperature using a computerized servohydraulic fatigue machine with a loading ratio K_{min}/K_{max}, (where K_{min} and K_{max} are calculated from the minimum and maximum applied load, respectively) equal to 0.4 at a frequency of 10 Hz. Three tests were conducted on X52 steel and two tests were conducted on Grade B steel.

The stress intensity factor range ΔK was calculated according to the following equation from Tada et al. [20]:

$$\Delta K = \frac{\Delta P}{BW}\sqrt{\pi(R_i\theta)}\cdot F(\theta),$$

$$F(\theta) = 1 + 7.5\left(\frac{\theta}{\pi}\right)^{3/2} - 15.0\left(\frac{\theta}{\pi}\right)^{5/2} + 33.0\left(\frac{\theta}{\pi}\right)^{7/2},$$

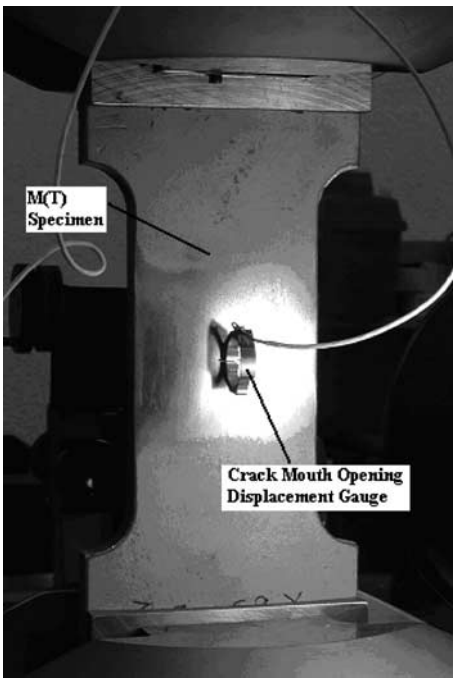

FIG. 4—*Experimental setup with CMOD gauge location.*

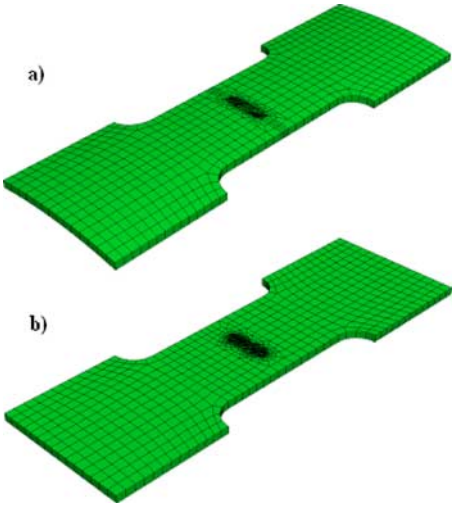

FIG. 5—*FE model of (a) curved and (b) flat M(T) specimen with 20 mm crack.*

$$\theta = \tan^{-1}\left(\frac{a}{R_i}\right), \tag{2}$$

where:

a = half crack length,
θ = crack half-circumferential angle,
R_i = mean radius (R_i = (OD/2)-(pipeline thickness/2)),
ΔP = applied load range, and
W and B = specimen width and thickness, respectively.
This equation is valid when $\theta < 110°$ [20].

A computer controlled K-increasing test, where the stress intensity is controlled as a function of the crack length, was used with a normalized K-increasing gradient equal to 0.1 (mm^{-1}). The initial ΔK was selected to be 90 $MPa \cdot mm^{1/2}$. To minimize fatigue crack tip damage (due to overload or underload), the initial precracking procedure was performed at a value of ΔK close to the actual testing value. The end test criterion was set to be either a crack growth rate of 5×10^{-2} mm/cycle or a half crack length of 36 mm (70 % of the M(T) specimen width.)

Influence of the M(T) Specimen Curve Shape

The FCGR tests were performed using the standard ASTM E647-05 [18], designed for flat M(T) specimens. To examine the effect that the M(T) curved specimen geometry had on the fatigue crack growth test results, finite element models of both the curved specimen and a corresponding flat specimen were developed in ABAQUS/STANDARD V6.6 general purpose FEA software [21]. Figure 5(*a*) shows the curved model, while Fig. 5(*b*) shows the flat model.

This comparison was performed with both the curved and flat models having the same thickness. However, the width at the ends on the flat plate was adjusted so the model had the same cross-sectional area as the curved model. This ensured that the same pressure loading on the flat model end corresponded to the same maximum load on the curved model end. As an additional verification, the difference in cross-sectional area of the gage section was measured between flat and curved models and found to differ by only 0.4 % for the Grade B model and 1.7 % for the X52 model.

Figure 6 details the boundary conditions applied on the model. In the figure, the boundary conditions applied are shown by the arrows, which indicate the constraint direction of these sections. The following constraints are applied to the model:

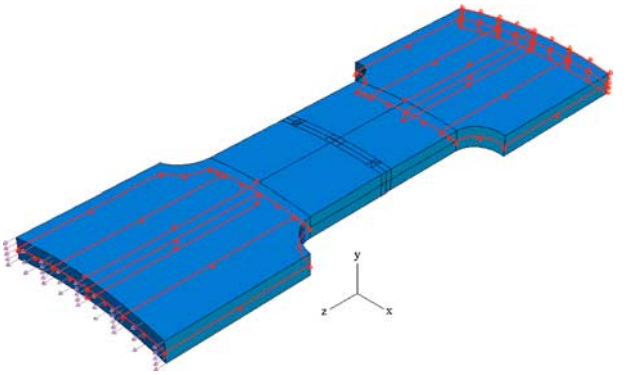

FIG. 6—*Boundary conditions applied to the finite element model.*

(a) At one end, a pressure load corresponding to a maximum force of 130 kN applied during actual testing is applied.
(b) At the opposite end of the model, the displacement in the Z-direction is fixed, corresponding to the fatigue test setup (e.g., Fig. 4).
(c) Additionally, boundary conditions were applied along the midsurface of the 152×126 mm^2 end section to restrict out-of-plane (Y-direction) displacement.
(d) Finally, along the centerline of the 152×126 mm^2 end sections, the X-direction displacement is fixed.

These last two constraints simulated the constraint imposed on the ends by the adaptor blocks (Fig. 3) and clamping force in the test machine. Using a displacement boundary condition along the midsurface of the model rather than trying to simulate the actual clamping forces on the adaptor blocks simplified the model, which was advantageous since numerous simulations were performed.

To verify these boundary conditions, a comparison was made to a FE model with the actual adaptor blocks included in the model, and the results were identical. Eliminating the adaptor blocks from the model improved the computational efficiency of the model.

20-node quadratic reduced-integration brick elements were used to mesh the models. Due to the specimen curvature, different meshing algorithms are required for the flat and curved specimens remote of the crack tip. This results in different mesh sizes along the specimen edges. However, similar meshing used around the crack tip prevents any element size dependencies. Mesh convergence was investigated by varying the element length from 0.25 to 3.0 mm. It was found that the CMOD values predicted by the model varied a maximum of 0.13 % over the range of mesh sizes. From this analysis, a mesh size of 1 mm was selected around the crack tip since it is less expensive computationally than the smaller elements and provides adequate ability to mesh the different crack lengths without excessive mesh distortion.

Singularities with single-node degeneracy and midside node placement of 0.5 along the element edge length were incorporated at the crack tips in the model [21]. Adjusting the singularity parameters did not significantly affect the CMOD results, so the above recommended parameters were used.

To predict the compliance relationship for each model, the crack length in the models was varied from 8 to 36 mm in increments of 4 mm. The CMOD predicted from the model, identified as the relative displacement across the notch edges along the center line of the

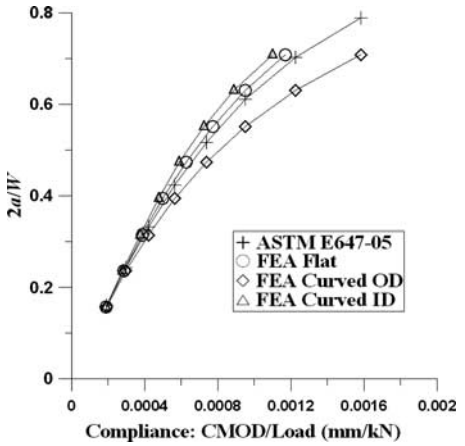

FIG. 7—*Curved and flat FE model results for X52 grade steel compared to ASTM [18] prediction for an applied load of 130 kN.*

model, corresponded to the CMOD gage attachment points in the experimental tests.

Whereas by symmetry the CMOD is the same for both sides of the flat specimen, the pipe curvature causes the CMOD to vary between the outer diameter (OD) and inner diameter (ID) of the curved model. The results for the flat plate model and both the ID and OD results of the curved plate model are plotted in Fig. 7 (for the X52 steel) and Fig. 8 (for the Grade B steel), for an applied load of 130 kN, along with the ASTM E647-05 expression used to predict the crack length as a function of compliance,

$$\frac{2a}{W} = C_1 x + C_2 x^2 + C_3 x^3 + C_4 x^4, \tag{3}$$

where:

a=half crack length,

W=specimen width,

C_1, C_2, C_3, and C_4=compliance coefficients (C_1=1.069 05, C_2=0.588 106, C_3=−1.018 85, C_4=0.361 691), and

x is calculated as

$$x = 1 - e^{(-\sqrt{(EBC_M+\eta)(EBC_M-\eta+c_1\eta+c_2\eta^{f3})})/2.141}, \tag{4}$$

where:

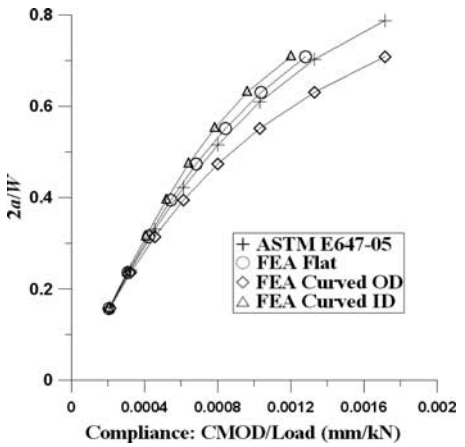

FIG. 8—*Curved and flat FE model results for Grade B steel compared to ASTM [18] prediction for an applied load of 130 kN.*

TABLE 6—*ASTM expression parameters.*

Parameter	X52	Grade B
W (mm)	101.6	101.6
B (mm)	8.1	7.4
L (mm)	152.4	152.4
E (MPa)	2.11×10^5	2.12×10^5
y (mm)	0.254	0.254

E=Young's modulus,

B=specimen thickness,

C_M=measured compliance (CMOD/load), and

$\eta = 2y/W$, where y is the distance from the crack to the point where the CMOD is measured (half of the gauge length) [18]. Table 6 summarizes the parameters used to calculate the ASTM expression (where L is the center uniform specimen length), and Fig. 2(a) presents these parameters in the ASTM drawing [18]. Because the test specimens are loaded uniformly at the ends, the values of c_1, c_2, and c_3 are taken as zero. The FEA verified that using the c_1, c_2, and c_3 corrections for both the pinned and clamped configurations produced crack length predictions nearly identical as those with $c_1 = c_2 = c_3 = 0$ for this particular geometry and loading situation.

The FEA simulations were performed with two different applied loads, 50 and 130 kN, in order to have a large range of relative crack length ($2a/W$) vs compliance relationship. In Figs. 7 and 8 only the results from the 130 kN are presented because the trend for the 50 kN simulations is similar due to linear elasticity theory.

From Figs. 7 and 8, the finite element results for both the flat specimen and the curved specimen differ slightly from the ASTM prediction for both steels. Figure 9 shows the percent difference between the known crack length in the FE simulations and the crack length predicted by the ASTM equation.

The difference between the flat FE model predictions and ASTM expression predictions is within 2 %. Several ideas about the cause of the discrepancy between the ASTM equation and the FE predicted model were explored. First, it was thought that while the FE models are three-dimensional, the ASTM equation is formulated from a plane stress relation. To explore this difference a 2D plane stress model with the same geometry as the 3D model was

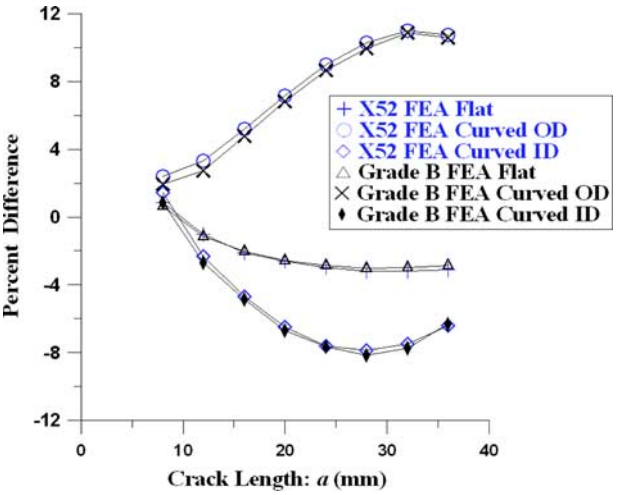

FIG. 9—*Percent error of ASTM crack length predictions compared to set FEA crack lengths.*

TABLE 7—*Compliance coefficients for the X52 and Grade B steels.*

Compliance Coefficients	C_1	C_2	C_3	C_4
ASTM E647-05	1.069,05	0.588,106	−1.018,85	0.361,691
X52 flat	0.990,23	1.203,53	−2.122,16	1.009,62
X52 curved (OD side)	1.073,75	0.420,78	−1.442,40	0.955,90
X52 curved (ID side)	0.935,47	1.475,79	−1.711,03	−0.012,19
Grade B flat	1.002,71	1.157,25	−2.048,42	0.956,81
Grade B curved (OD side)	1.084,15	0.419,21	−1.477,63	0.990,50
Grade B curved (ID side)	0.923,86	1.768,28	−2.620,75	0.750,36

created. It yielded the same results as the flat 3D model and was thus not the source of the discrepancy.

Further, it was also thought that using the CMOD in the compliance calculation might affect the crack length predictions, so two different y values, $y=6.75$ mm and $y=20.9$ mm from the crack plane, were used to predict the crack length in the model. Using these two alternate points yielded nearly identical crack length predictions from the ASTM expression as those obtained from using the CMOD, $y=0.254$ mm, as the point of evaluation.

In reality, the ASTM expression is a polynomial fit of the Eftis and Liebowitz expression [22] and has been developed to take into account a range of specimen geometries; some small variance in the crack length predictions is therefore expected.

Examining the curved results in Fig. 9, the ASTM expression generally underpredicts the crack length for long cracks in comparison with the flat and curved ID simulations and overpredicts the crack length for long cracks in the comparison with curved OD simulations. The difference in compliance between the OD and ID FE predictions, as crack length increases, is likely due to the displacement of the specimen's cross-sectional centroid relative to the loading axis. As the remaining ligament decreases, the specimen's halves rotate. These differences and their consequences on fatigue life predictions will be discussed later.

At this point in this study, it is clear that the ASTM expression, while valid for flat specimens, could not accurately predict the crack length for this particular curved geometry and loading situation, but the repercussion of the different crack length calculations on fatigue life predictions remains unknown. To explore this, new empirical coefficients for the ASTM expression were calculated based on the curved FEA compliance results. Table 7 presents the corrected compliance coefficients for the X52 and Grade B steels. These coefficients will be used in the experimental fatigue results section of this paper.

Experimental Results and Discussion

Figure 10 presents the FCGR curves for the pipeline steels X52 and Grade B using the ASTM E647-05 [18] method, with the original parameters to calculate the compliance relationship, and Eq 2 to calculate the stress intensity factor. In this figure, two FCGR test results are plotted for the Grade B and three for the X52.

The two FCGR curves for the tested steels show similar trends. Minor differences are observed at the beginning of the propagation. At the end the FCGR propagation, corresponding to region III, the two curves begin to diverge slightly. This divergent behavior reflects the fact that the microstructure of the steel influences the failure mechanisms more than the fatigue mechanisms in this higher loading regime.

From the FEA study, two new FCGR curves were plotted for each steel. The first curve, for the flat specimen model, presents a crack length estimation based on CMOD measurements from the fatigue test and the compliance coefficients calculated from the FEA results (third row, for the X52 steel, and sixth row, for the Grade B steel, in Table 7). The second curve presents a crack length estimation based on the CMOD measurements and the compliance coefficients calculated from FEA results obtained for the curved (OD side) specimen model (fourth row, for the X52 steel, and seventh row, for the Grade B steel, in Table 7). Figure 11 compares these FCGR curves for the two steels. For these curves, ΔK was determined using the equation of Tada et al. [20] (Eq 2) with the

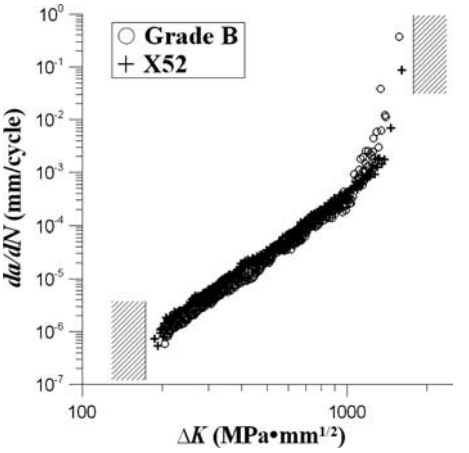

FIG. 10—*FCGR curves for the X52 and Grade B steels.*

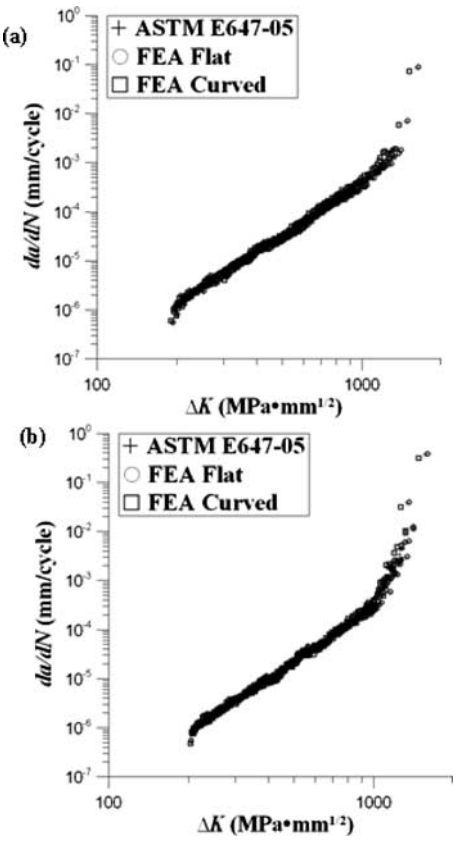

FIG. 11—*FCGR curves calculated with three different crack length estimations for the (a) X52 and (b) Grade B steels.*

TABLE 8—*Statistical results for all the FCGR curve determinations.*

Designation	m	ln(C) [a]	Mean C	Mean C+2 SD	SD/Mean C (%)	Number of Points Used
X52 ASTM E647-05	3.49	N(−44.08;0.12)	1.22×10^{-14}	1.54×10^{-14}	13.1	180
X52 flat	3.44	N(−43.68;0.12)	1.58×10^{-14}	1.99×10^{-14}	13.0	179
X52 curved (OD side)	3.51	N(−44.29;0.12)	1.06×10^{-14}	1.34×10^{-14}	13.2	181
Grade B ASTM E647-05	3.67	N(−46.15;0.11)	2.88×10^{-15}	3.58×10^{-15}	12.2	166
Grade B flat	3.60	N(−45.80;0.11)	3.60×10^{-15}	4.48×10^{-15}	12.2	164
Grade B curved (OD side)	3.69	N(−46.33;0.11)	2.56×10^{-15}	3.20×10^{-15}	12.5	166

[a] ΔK is expressed in MPa·m$^{1/2}$.

Note: SD is the standard deviation, the letter N is the normal distribution, the first number after the letter N refers to the mean, and the second refers to the standard deviation (in the ln(C) column, ΔK is expressed in MPa·m$^{1/2}$ as usually mentioned in RBI [24] but remained expressed in MPa·mm$^{1/2}$ in the other columns.

new crack length values. The ΔK values obtained with the Tada et al. equation are very close to those given by the ASTM E647-05 ΔK equation [18]. This is not surprising because the stress intensity factors were analyzed for flat and curved specimen configurations in the FEA models, and a small influence of the curvature was observed. This is easily understood by the fact that the stress intensity at the crack tip is more highly influenced by the sharpness of the crack than by the specimen curvature. The specimen curvature affects the stress field only slightly in comparison to the effect of the crack, especially when the pipeline diameter is large, which is the case in the present study.

From the statistical point of view, when the Paris law is used, m is fixed and C is used to represent the scatter [8,23]. The determinist choice of the m parameter, presented in standard BS 7910 [8], is due to the fact that the results obtained by considering m as a random variable cannot be transposed from laboratory accelerated conditions to service conditions (this is due to the nonlinearity caused by the Paris law m). The distribution of ln(C) is assumed to be normally distributed (as the fatigue life is assumed log-normally distributed). Similar to the approach used in risk based inspection (RBI), we make these assumptions to evaluate the scatter in the crack growth rate results [24]. This approach is valid if the individual estimates of C are independent (the population of C needs to be statistically independent; otherwise, we could not consider that the data are independent and we could not perform a statistical analysis of C).

In the stable crack growth region, a statistical study of the C parameter was conducted, assuming each of the FCGR test points was independent. The parameter m was taken as the mean value, and the parameter C was calculated for each FCGR test point. Table 8 summarizes the statistical results for the steels. In Table 8, SD is the standard deviation, the letter "N" is the normal distribution, the first number after the letter N refers to the mean, and the second refers to the standard deviation (in the ln(C) column in Table 8, ΔK is expressed in MPa·m$^{1/2}$ as usually mentioned in RBI [24] but remained expressed in MPa·mm$^{1/2}$ in the other columns of the table). The "Mean C+2 SD" column represents the fatigue crack growth law upper bound parameter used in FCGR design, as seen in the BS 7910 standard [8]. These statistical results are determined in region II of the fatigue crack growth (stable crack growth). Figure 12 shows that the scatter of the parameter C for crack length determination, based on FEA curved specimen (OD side) simulations for each steel, is random. Similar results were found for all FCGR curve determinations presented here. From Figs. 11 and 12 and from Table 8, several remarks can be made.

(1) In Fig. 12, the scatter of the parameter C shows no trend, confirming the statistical independence of C. The standard deviation of C is a small fraction of the mean values.

(2) The FCGR curves obtained using the ASTM E647-05 [18] and the FEA results are similar. Table 8 showed similar results between ASTM and FEA Paris parameters. In order to investigate the difference in the fatigue crack growth results, a comparison is made for a crack growing from a length of 0.5 mm and increasing up to a length of 5.0 mm. These example depths were chosen to keep ΔK in region II (linear Paris law region) from initial to final crack lengths in order to be focused only on the fatigue properties. The initial crack length, 0.5 mm, with an initial da/dN higher than 10^{-6} mm/cycle, avoids any influence from the early fatigue stage. The final crack length, 5.0 mm, is reached before any critical crack length for steel failure, thus avoiding any influence of material toughness and plasticity. The

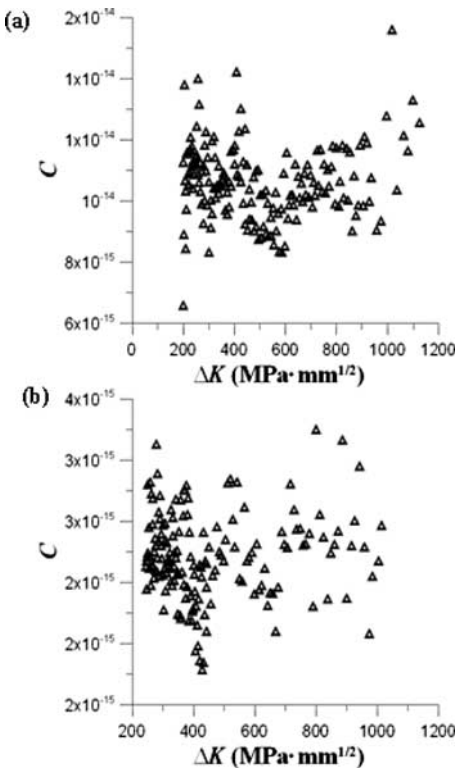

FIG. 12—*Scatter of the parameter C using FEA curved specimen (OD side) models for (a) X52 and (b) Grade B steels.*

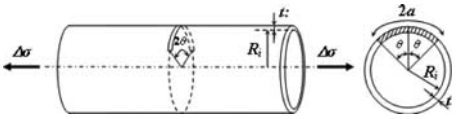

FIG. 13—*Sketch of the pipeline application example, with crack geometry, used in fatigue lifetime comparisons.*

TABLE 10—*Comparison of the final fatigue crack length (a in mm).*

Designation	Measured from the Test	ASTM E647-05	FEA Flat	FEA Curved (OD Side)
X52	28.7	33.3	34.7	30.0
Grade B	24.0	33.2	34.2	29.7

focus is on predicting the range in service life characteristic of a pipeline containing a flaw and having relatively small variations in FCGRs. As application example a pipeline with a through-thickness flaw (Tada et al. [20] case for the ΔK calculation of Eq 2), with a uniform applied loading range $\Delta\sigma$ equal to 80 MPa (with a stress ratio equal to 0.4 as in the FCGR tests), and with same dimensions as the Grade B pipeline was assumed. A sketch of the example is presented in Fig. 13, showing the through-thickness flaw. The results of these simulations are presented in Table 9. From Table 9 several remarks can be made. ASTM E647-05 shows similar fatigue life trends to those calculated using the FEA compliance relationships. The flat simulations are slightly more conservative than the curved simulations due to an overestimation of the crack length in the final part of the fatigue crack growth propagation in the FEA curved simulations. We note that all the fatigue life calculations are within approximately 10 % of the ASTM prediction.

(3) The steels tested had significant differences in microstructure (banding) but show little difference in fatigue properties. This result is not surprising particularly when the initiation and final stages of fatigue are not considered. The ferrite-pearlite pipeline steel without banding (Grade B) has slightly better FCGR properties than the ferrite-pearlite pipeline steel with banding (X52).

(4) In order to verify the accuracy of the crack length estimation presented here, the final crack lengths predicted using the FE compliance relationship is compared to the final crack lengths measured from the tests. This comparison is shown in Table 10.

From Table 10, the FEA curved (OD side) simulation leads to a better final crack length estimation than ASTM E647-05 and FEA flat simulations, which lead to similar results. The use of the FEA curved (OD side) simulation appears to be more accurate.

Conclusions

The fatigue behavior of two pipeline steels was investigated. Curved M(T) (full-thickness) fatigue specimens were used. The specimens were machined directly from the pipeline along the longitudinal orientation (L-C orientation). FEAs were carried out to show the M(T) curvature effects on the FCGR results for two different pipeline steels.

Experimental results show minor differences in FCGR between the two ferrite-pearlite, 0.2–0.3 wt % carbon steels. The ferrite-pearlite pipeline steel without banding (Grade B) has a slightly better fatigue resistance than the ferrite-pearlite pipeline steel with banding (X52).

Uncertainty in the FCGRs was analyzed by attributing all the scatter in FCGR to the Paris law parameter *C*. The standard deviation of the *C* parameters was a small fraction of the mean values. Uncertainties in the FCGRs produced quite small standard deviations in the predicted lifetimes. The flat and curved (OD) life predictions are particularly close, thereby indicating that the predictions based on the flat specimen are only slightly nonconservative and may be adequate for most applications. Considering the uncertainties in the predicted range of lifetime (for example, the range between the mean value and the mean plus two standard deviations), the similarities of the predicted lifetimes for the two steels tested were confirmed.

The ASTM E647-05 compliance relationship [18] accurately predicts the crack length for a particular geometry and loading situation. The FEA flat and curved compliance relationships demonstrate trends similar to those seen in the ASTM standard. Finally, the FEA compliance relationship curve seems to be the most accurate based on the actual final crack length estimations but has only a slight influence on the fatigue life calculation (difference of 10 %). These observations showed that the ASTM polynomial compliance equation (Eq 3) can accurately be used for M(T) specimens (flat and/or with different pipeline curvatures) using ASTM E647-05 coefficients.

Acknowledgments

The support of Pacific Gas and Electric is gratefully acknowledged for contributing the pipeline steel and for the permission to publish this work. The support of the U.S. Department of Transportation, Pipeline and Hazardous Materials Safety Administration is appreciated. The efforts of Dr. Richard E. Ricker, Metallurgy Division, NIST, for conducting dynamic Young's modulus measurements on the pipeline steels are also appreciated.

TABLE 9—*Fatigue life calculated for a crack depth growing from 0.5 to 5.0 mm (mean and* mean±2 SD*).*

Life Duration (cycles)	Designation					
	X52 ASTM E647-05	X52 flat	X52 curved (OD side)	Grade B ASTM E647-05	Grade B flat	Grade B curved (OD side)
Mean−2 SD	2.55×10^6	2.43×10^6	2.63×10^6	4.29×10^6	4.12×10^6	4.41×10^6
Mean	3.22×10^6	3.07×10^6	3.33×10^6	5.33×10^6	5.13×10^6	5.51×10^6
Mean+2 SD	4.07×10^6	3.86×10^6	4.22×10^6	6.63×10^6	6.38×10^6	6.90×10^6

References

[1] Kunert, H. G. and Otegui, J. L., "Factors Influencing Transit Fatigue of Seamless Pipes," *Fatigue Fract. Eng. Mater. Struct.*, Vol. 28, 2005, pp. 455–466.

[2] Bruno, T. V., "How to Prevent Fatigue to Tubular Goods," Standardiztion Confernce fo the Production Department, American Petroleum Institute, New Orleans, LA, 1987, http://www.metallurigical.com/Publications/Publication%2022.pdf.

[3] Jaske, C. E., "The Effect of Cathodic Polarization on Fatigue Behavior," *Proceedings of the Annual Conference and Exhibition on Corrosion*, Paper No. 03243, San Diego, CA, 2003, NACE, Houston, TX.

[4] Kiefner, J. F., Kolovich, C. E., Zelenak, P. A., and Wahjudi, T., "Estimating Fatigue Life for Pipeline Integrity Management," *Proceedings of the 5th International Pipeline Conference*, Paper No. 0487, Calgary, Alberta, Canada, 2004, ASME, New York.

[5] Vosikovsky, O., "Fatigue Crack Growth in X65 Line-Pipe Steel at Low Cycles Frequencies in Aqueous Environments," *J. Eng. Mater. Technol.*, Vol. 97, 1975, pp. 298–304.

[6] "Structural Integrity Procedures for European Industry," *Structural Integrity Procedure for Europe*, SINTAP, 1999.

[7] American Society of Mechanical Engineers, 1990, "Rules for In-Service Inspection of Nuclear Power Plant Components, Section XI, Appendix H, Evaluation of Flaw in Ferritic Piping, Addenda, ASME eds.," *ASME Boiler and Pressure Vessel Code*, New York, NY.

[8] BS 7910, "Guide to Methods for Assessing the Acceptability of Flaws in Metallic Structures," BSI, Eds., British Standards Institution (BSI), London, United Kingdom, 2005.

[9] API RP 579, "Recommended Practice for Fitness-for-Service," API, Eds., American Petroleum Institute, Washington, DC, 2000.

[10] Vosikovsky, O. and Rivard, A., "Growth of Surface Fatigue Cracks in Steel Plate," *Int. J. Fatigue*, Vol. 3, 1981, pp. 111–115.

[11] Vosikovsky, O., "Effect of Stress Ratio on Fatigue Crack Growth Rates in X70 Pipeline Steel in Air and Saltwater," *J. Test. Eval.*, Vol. 8, No. 2, 1980, pp. 68–73.

[12] Vosikovsky, O., "Fatigue Crack Growth in X70 Line-Pipe Steel in Sour Crude Oil," *Corrosion (Houston)*, Vol. 32, No. 12, 1976, pp. 472–475.

[13] Shi, Y. W., Chen, B. Y., and Zhang, J. X., "Effects of Welding Residual Stresses on Fatigue Crack Growth Behaviour in Butt Welds of a Pipeline Steel," *Eng. Fract. Mech.*, Vol. 36, 1990, pp. 893–902.

[14] Xiong, Q. R., Zhuang, C. J., Feng, Y. R., Li, L. K., and Huo, C. Y., "Experimental Studies on Fatigue Crack Growth Characteristics of X65 SSAW Pipe," *Proceedings of the Seventh International Fatigue Congress*, Beijing, China, June 8–12, 1999, EMAS, Wartley, UK.

[15] Hagiwara, N., Masuda, T., and Oguchi, N., "Effects of Prestrain on Fracture Toughness on Fatigue-Crack Growth of Line Pipe Steels," *J. Pressure Vessel Technol.*, Vol. 123, 2001, pp. 355–361.

[16] Hillenbrand, H.-G., Liessem, A., Knauf, G., Niederhoff, K., and Bauer, J., "Development of Large-Diameter Pipe in Grade X100—State-of-the-Art Report from the Manufacturer's Point of View," *Proceedings of the Third International Pipeline Technology Conference*, Vol. 1, R. Denys, Ed., Brugge, Belgium, May 21–24, 2000, Elsevier, New York, pp. 169–482.

[17] ASTM Standard E1876-07, 1998, "Standard Test Method for Dynamic Young's Modulus, Shear Modulus, and Poisson's Ratio by Impulse Excitation of Vibration," *Annual Book of ASTM Standards*, Vol. 03.01, ASTM International, West Conshohocken, PA.

[18] ASTM Standard E647-05, 1998, "Standard Test Method for Measurement of Fatigue Crack Growth Rates," *Annual Book of ASTM Standards*, Vol. 03.01, ASTM International, West Conshohocken, PA.

[19] ASTM Standard E1823-05a, 1998, "Standard Terminology Relating to Fatigue and Fracture Testing," *Annual Book of ASTM Standards*, Vol. 03.01, ASTM International, West Conshohocken, PA.

[20] Tada, H., Paris, P. C., and Irwin, G. R., *The Stress Analysis of Cracks Handbook*, 3rd ed., American Society of Mechanical Engineers, New York, NY, 2000.

[21] Abaqus Standard/User's Manual v6.6, 2007, Hibbitt, Karlsson, and Sorensen, Inc., Providence, RI, www.abaqus.com.

[22] Eftis, J. and Liebowitz, H., "On the Modified Westergaard Equations for Certain Plane Crack Problems," *Int. J. Fract. Mech.*, Vol. 8, 1972, pp. 383–391.

[23] Darcis, Ph. P., Santarosa, D., Recho, N., and Lassen, T., "A Fracture Mechanics Approach for the Crack Growth in Welded Joints with Reference to BS 7910," *Proceedings of the 15th European Conference of Fracture*, Stockholm, Sweden, 2004, ICTH, Stockholm.

[24] Kirkemo, F., "Applications of Probabilistic Fracture Mechanics to Offshore Structures," *Appl. Mech. Rev.*, Vol. 41, 1988, pp. 61–84.